Nuclear Instruments and Methods in Physics Research A268 (1988) 561–566
North-Holland, Amsterdam

DESIGN OF A TANDEM ACCELERATOR FREE ELECTRON LASER +

I. BEN-ZVI, A. GOVER *, E. JERBY *, J.S. SOKOLOWSKI and J. WACHTEL **

Department of Nuclear Physics, The Weizmann Institute of Science, Rehovot 76100, Israel

The motivation for using a tandem electrostatic accelerator as an electron accelerator for a free electron laser (FEL) is presented. The adaptation of the HVEC EN tandem at the Weizmann Institute for this purpose, electron beam optics and nonlinear FEL computation relevant for this FEL realization are described. In the tandem configuration the terminal is held at a positive potential. The electron beam is accelerated from ground potential to the terminal in one beam tube and then decelerated down the other beam tube. The FEL wiggler and cavity are at the terminal. Due to the beam energy recovery this scheme produces a high power beam at the terminal with a small investment in electrical power.

1. Introduction

The tandem electrostatic accelerator at the Weizmann Institute of Science (a HVEC model EN) is being modified for high current electron acceleration followed by deceleration. The purpose of this conversion is the construction of a free electron laser (FEL) based on this accelerator [1]. The project is carried out by a collaboration of research groups from the Applied Physics Department at the Israeli Ministry of Defence, Faculty of Engineering at the Tel Aviv University and the Nuclear Physics Department at the Weizmann Institute of Science.

Most FEL projects in the optical frequency regime were based so far on rf accelerators (storage rings, linacs or microtrons) or induction accelerators. A unique scheme, based on a Van de Graaff accelerator, was demonstrated recently by the UCSB group, headed by Elias [2]. They succeeded in demonstrating the operation of such an accelerator with long pulses (tens of microseconds) of high current (1 A) by using a beam energy retrieval method. In this scheme the high power of the laser is supplied by a moderate voltage high current collector power supply, and the accelerator charging system need only supply enough current to compensate for beam current loss in the HV terminal or acceleration tubes. The depressed collector scheme used in microwave tube techniques enables the operation of devices with radiative extraction efficiency beyond 50%. Such high efficiencies and correspondingly high laser power would seem highly attractive for a coherent optical source.

The two significant properties of an electrostatic accelerator as an FEL electron beam source are the high quality of in the beam and the long pulse duration (possibly continuous operation). The significance of a high quality electron beam in determining the limits of FEL operating parameters has been the subject of a detailed quantitative analysis [3,4]. The characteristics of any radiation device which is composed of many infinitesimal radiators (like atoms or elctrons) are dependent on the statistical parameters of the radiators. It can be shown, that in this sense the FEL has a significant advantage over atomic lasers, since an electron beam constitutes an ensemble of radiators which is highly dense in phase space and can thus produce high brightness spontaneous emission radiation sources (undulator radiation), as well as stimulated emission sources with high gain, high radiative energy extraction efficiency. The performance of these devices at short (optical) wavelength is fundamentally limited by the statistical distribution (beam quality) parameters of the electrons.

Another aspect of the electrostatic accelerator – the possibility of long pulse duration (possibly CW operation) also results in unique advantages. If the inherent high quality of the beam is retained, high current (tens of amperes) and long pulses of radiation may be obtained with an FEL based on an electrostatic accelerator. This gives the opportunity to study post-saturation effects (stability, spectral side bands) and efficiency enhancement schemes like temporal tapering (ramping) of FEL parameters. The long pulse and high current may also be of interest in some applications, since it produces radiation with high quasi-CW average power (in contrast to high peak power in RF accelerators with micropulse structure).

+ Supported in part by a grant from Yeda Research and Development Co. Ltd.

* Faculty of Engineering, Tel-Aviv University, Ramat-Aviv 69978, Israel.

** Elta Electronics Industries, Ashdod, Israel.

0168-9002/88/$03.50

2. The tandem accelerator

Fig. 1 shows the electron beam optics. The wiggler is inside the accelerator in the HV terminal, and the electron gun and beam collector are at the (negative) cathode voltage of 50 kV. The electrons are accelerated towards the positive terminal in one acceleration tube. In the wiggler about 20 keV (average per electron) is extracted through the FEL interaction. Then the beam is decelerated in the other tube. There is a broad spectrum of energies for the collected electrons. Bringing all these electrons back to the potential of the gun cathode requires power investment at the collector, and this is the power which is actually transferred to the optical radiation field.

The electron beam optics in this scheme is simple with no bends other than those produced by the wiggler. There is also good accessibility to the electron gun, collector and their associated electronics at the expense of limited accessibility and limited space for the wiggler. With this nearly straight line electron optics, good current collection efficiency may be exercised, enabling longer pulse duration and higher current levels.

The electron beam optics components of the tandem are shown in fig. 1. Vacuum pump connections, valves and instrumentation connections are not shown, but they affect the beam optics design.

The gun was designed using Herrmannsfeldt's electron trajectory program [5]. The design principle follows the UCSB approach. Starting with a large area cathode with weak focussing in the gun, one obtains a beam which does not spread too fast on account of space charge. The control electrode is ungridded for best emittance. The emittance calculated for the gun is completely dominated by thermal spread. The current is 1.7 A at a control electrode voltage of 12 kV and the optimum anode voltage is 50 kV.

The lens system between the gun and the acceleration tube keeps the beam from growing radially too much and provides focus adjustment at the wiggler position. The output beam from the gun was followed through the lens section using the Herrmannsfeldt code and it was verified that magnetic focussing by current loop lenses does not increase the emittance of the beam significantly, provided one uses a large enough diameter of the current loop. With the beam predicted by the numerical model of the gun, at 1.7 A, lenses of less than 2000 ampere-turns with a current loop diameter of 25 cm provides a good transport system for this beam. The lens separation is about 50 cm for a beam diameter that varies between 3 cm to 6 cm.

The entrance to the acceleration tube (as well as the exit from the deceleration tube) act as rather strong lenses. The electrode system of the tube has an inner diameter of 5 in. It was found that in order to avoid aberrations at the entrance lens, the beam diameter should be kept under 6 cm. To get a beam waist at the wiggler the tube entrance lens has to be augmented by an additional lens.

As one can see in fig. 1, the acceleration tubes are inclined to fit the wiggler at its natural injection angle [1], which is approximately 7° for our particular choice of electron energy and wiggler strength. Since the wiggler is 1 m long, while the tube assembly is about four times longer (on each side), the tubes inclination with respect to the tank axis is less than 0.9°.

The main advantage of this arrangement is that the optical beam axis and the electron beam axis are separated. Fig. 1 shows a set of deflection plates, two small correction electromagnets (at each end of the wiggler) and three sets of (nondestructive) beam position monitors, at both ends of the wiggler and before the collector. This instrumentation supplies information and control for getting the beam correctly in and out of the wiggler and the tandem and to correct for the fringe fields of the wiggler.

Fig. 2 shows the electrical layout of the accelerator. For the depressed collector scheme, the gun cathode and the main collector element are essentially at the same potential. Electrons which do not strike an obstacle deposit very little energy at the collector, even for a 1 to 2 A beam. The only current which the electron beam draws (in the steady state) from the 50 kV gun supply or from the tandem charging system is the beam current loss due to interception at places other than at the collector.

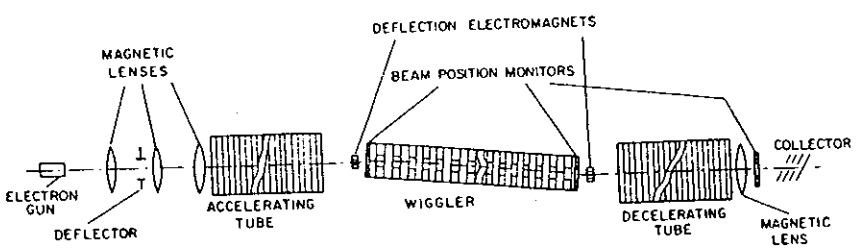

Fig. 1. Schematic diagram of the tandem FEL electron beam optics.

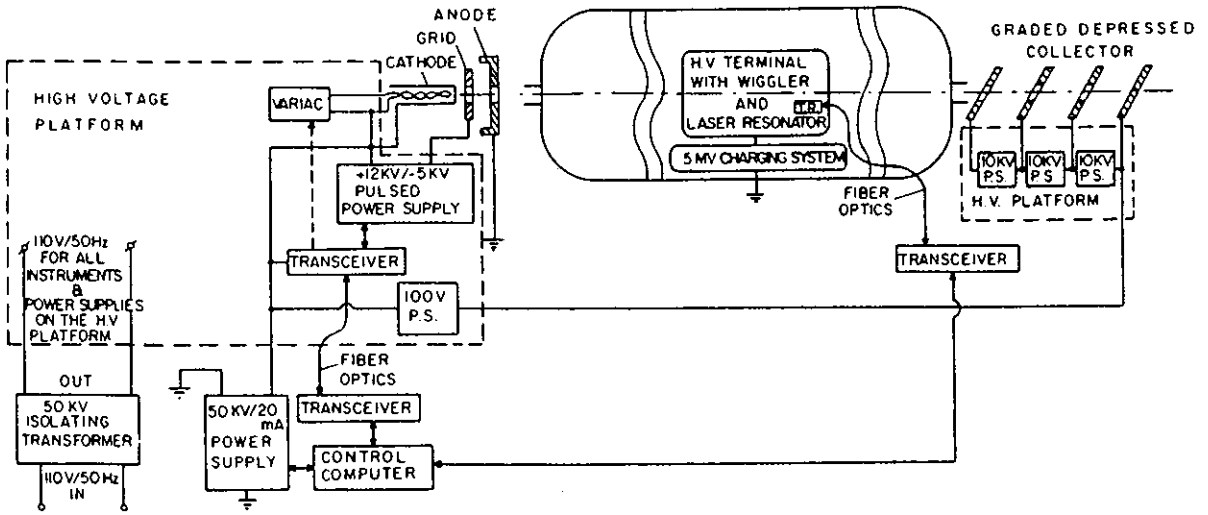

Fig. 2. Block diagram of the tandem FEL electrical circuit.

With the FEL lasing, an energy spread is imposed on the electron beam and a fraction of the beam will be collected at lower potentials on the multistage collector electrodes. Thus the FEL optical beam power will be restored by the 10 kV collector power supplies. With the laser off but the electron beam on, the power consuption is negligible due to the depressed collector arrangement. Special care is required in the design of the collector end because of the large energy spread in the beam.

The control electrode power supply (pulsed voltage from -5 kV for current cut off to $+12$ kV), the cathode heater variac, the collector power suplies as well as control and instrumentation electronics are placed on a high voltage platform, at -50 kV. Electrical ac power to the platform is supplied through an isolation transformer. The electronics on the gun platform and the tandem terminal will be controlled via fiber optics links connected to a microcomputer.

3. Nonlinear FEL computation and phase space matching

Using a tandem electrostatic accelerator as an electron beam source for an FEL introduces unusual beam optics problems. The finite phase space volume occupied by the electron beam limits the gain of the FEL which must exceed the minimum for oscillation threshold. On the other hand interaction with the coherent optical radiation generally expands the phase space of the electron beam affecting the ability to recover the beam in the collector. The present design effort treats these two effects by calculating the mutual interaction of the radiation and the electron beam distribution in a self consistent way.

In the first design area, the electron beam phase space acceptance of the FEL is determined based upon criteria for sustaining sufficient small signal gain. Detailed computations have been performed and the results are presented here. In the second area the phase space acceptance of the beam recovery system must be used as a factor that limits the nonlinear operating characteristics of the FEL. For fixed parameters that include the beam current, wiggler length, wiggler field strength, wiggler wavelength and optical wavelength, the saturated nonlinear steady state optical field intensity is mainly controlled by the reflection coefficient of the optical cavity mirrors. The intensity of the optical field that resonates with the electron motion in the wiggler determines the expansion of the phase space occupied by the beam as it passes through the FEL. The FEL must be designed to limit this phase space to the acceptance of the beam recovery system in the tandem accelerator. An exact computation of the electron motion in the optical radiation field and the wiggler magnetic field is required, and it must consider all of the three-dimensional features of the wiggler and radiation fields.

A computer program that tracks groups of electrons was written. It was applied to analyze an FEL model based on a symmetrical focusing planar wiggler of the kind proposed by Scharlemann [6] that is realizable by means of parabolic magnet pole face shaping. In the x–z wiggler plane the short wavelength wiggler motion is superimposed upon the long wavelength betatron oscillation, taking place due to the focusing effect of the curved magnetic pole faces. In the y–z plane mainly the standard betatron motion occurs. In the Scharlemann wiggler there is a unique orbit that has zero betatron oscillation amplitude. This is the reference orbit for the beam optics computations.

The optical radiation, at angular frequency ω, is polarized in the wiggler plane. When the ponderomotive wave, due to the beating between the wiggler field and the optical field, travels with phase velocity near the average axial electron velocity, the electron beam is bunched in the axial direction. Nonuniformity of the radiation field envelope or phase affects the resonance and can lead to reduced electron bunching among other complicated phase space phenomena.

A Fabry–Perot spherical mirror laser cavity sustains the radiation field. Analytic expressions for the symmetric Gaussian mode are used in the computation. It is assumed that only one linearly polarized, fundamental Gaussian mode is excited [7]. Confinement of the radiation field by the mirrors causes significant departures from infinite plane wave characteristics. In addition to the Gaussian amplitude dependence upon $r=(x^2+y^2)^{1/2}$ there is also wavefront curvature leading to a small axial component of the optical field. For practical values of mirror radius of curvature this component is negligible and it is ignored in the computation. Wavefront curvature also introduces a phase shift relative to a simple plane wave.

All of the above details are included in the computation to determine, for different sets of electron beam parameters, small signal gain spectra and the optical wave amplitude in the saturated steady state. A representative set of simulation electrons, initially distributed uniformly with respect to the phase ψ of the ponderomotive wave, generates the electron phase space statistics. The energy change of $\Delta\gamma mc^2$, the phase space coordinates x, y, z, p_x, p_y, p_z and the phase

$$\psi=(\omega/c+nk_W)z-\omega t, \qquad n=1,3,5,\ldots,$$

(where k_W is the wiggler wave-number) for each electron are recorded at the end of the wiggler field. In addition computer generated plots of x, y, $\Delta\gamma$ and ψ as functions of z give vivid graphic pictures of electron dynamics in the FEL. The average electron energy loss is calculated and identified with the energy transferred to the optical radiation field. When balanced by the transmission and diffraction loss of the cavity the amplitude defines the nonlinear, saturated steady state operating point of the FEL.

To check the accuracy of the program, parameters were adjusted to facilitate a comparison with analytical expressions [8]. The computed gain agreed well with the analytical results for the small gain, tenuous beam limit [1]. It should be noted that specifying the radiation field as the constant power empty optical cavity mode, implies the assumption of operating in the small gain, tenuous beam limit. The small gain limit is implicitly contained in the computation because the amplitude and frequency of the wave are considered to be constant during the transit time of a beam electron. The maximum single pass gain computed in the present study using the proposed FEL parameters was 8%.

Table 1
Values of proposed FEL parameters

	electron beam energy	5 MeV
I	electron beam current	1 A
B_W	wiggler field strength on the axis	0.63 T
λ_W	wiggler wavelength	0.024 m
L_W	wiggler length	1.008 m
λ	optical wavelength	67.55×10^{-6} m
R_c	cavity mirror curvature radius	0.91 m
L_c	cavity length	1.20 m
n	wiggler harmonic	3
Calculated constants		
W_0	optical cavity waist radius	3×10^{-3}m
a_W	wiggler parameter	1.4119

In table 1 the values of the proposed FEL parameters [1] that were used in the computations are listed.

The equations of motion are written below in terms of the normalized variables

$$P_\xi=p_x/mc, \quad P_\eta=p_y/mc, \quad P_\zeta=p_z/mc,$$

$$\zeta=k_W x, \quad \eta=k_W y, \quad \zeta=k_W z,$$

$$\psi=(\omega/c+nk_W)z-\omega t.$$

The normalized time variable $s=(eB_W/m)t$ is used so that $(\,)'\equiv \mathrm{d}(\,)/\mathrm{d}s$. The electromagnetic mode vector potential amplitude a is replaced by $A=ea/2mc$ and the wiggler strength by the wiggler parameter $a_W=eB_W/k_W mc$.

With these substitutions the equations of motion are

$$P_\xi'=-\frac{A}{a_W}\frac{\lambda_W}{\lambda}\frac{W_0}{W}e^{-r^2/W^2}(1-P_\zeta/\gamma)\cos[\psi-n\zeta-\theta]$$
$$-\frac{P_\eta}{\gamma}\sqrt{2}\cosh\frac{\xi}{\sqrt{2}}\sinh\frac{\eta}{\sqrt{2}}\sin\zeta$$
$$-\frac{P_\xi}{\gamma}\cosh\frac{\xi}{\sqrt{2}}\cosh\frac{\eta}{\sqrt{2}}\cos\zeta,$$

$$P_\eta'=\frac{P_\zeta}{\gamma}\sinh\frac{\xi}{\sqrt{2}}\sinh\frac{\eta}{\sqrt{2}}\cos\zeta$$
$$+\frac{P_\xi}{\gamma}\sqrt{2}\cosh\frac{\xi}{\sqrt{2}}\sinh\frac{\eta}{\sqrt{2}}\sin\zeta,$$

$$P_\zeta'=-\frac{A}{a_W}\frac{\lambda_W}{\lambda}\frac{W_0}{W}e^{-r^2/W^2}\frac{P_\xi}{\gamma}\cos[\psi-n\zeta-\theta]$$
$$+\frac{P_\xi}{\gamma}\cosh\frac{\xi}{\sqrt{2}}\cosh\frac{\eta}{\sqrt{2}}\cos\zeta$$
$$-\frac{P_\eta}{\gamma}\sinh\frac{\xi}{\sqrt{2}}\sinh\frac{\eta}{\sqrt{2}}\cos\zeta,$$

$$\xi'=\frac{P_\xi}{\lambda a_W}, \qquad \eta'=\frac{P_\eta}{\gamma a_W}, \qquad \zeta'=\frac{P_\zeta}{\gamma a_W},$$

$$\psi'=\frac{1}{a_W}\frac{\lambda_W}{\lambda}\left[\left(1+n\frac{\lambda}{\lambda_W}\right)(P_\zeta/\gamma)-1\right],$$

where

$$\gamma = \left(1 + P_\xi^2 + P_\eta^2 + P_\zeta^2\right)^{1/2}, \quad r^2 = x^2 + y^2,$$

$$W_0^2 = \frac{\lambda}{2\pi}\left[(2R_c - L_c)L_c\right]^{1/2}, \quad W^2 = W_0^2\left[1 + \left(\frac{\lambda z}{\pi W_0^2}\right)^2\right],$$

and

$$\theta = \tan^{-1}\left(\frac{\lambda z}{\pi W_0^2}\right) - \frac{\pi r^2}{\lambda R(z)}, \quad R(z) = z\left[1 + \left(\frac{\pi W_0^2}{\lambda z}\right)^2\right].$$

By introducing the seventh equation for the rate of change of the phase, ψ', it is possible to eliminate the time t (or s) from the RHS of all the equations. The construction of an electron sample representing a constant current electron beam is reduced trivially to specifying initial values of ψ distributed uniformly between 0 and 2π. Examining the first three equations it is easy to identify the driving terms due to the wiggler and to the optical field. The equations for P_ξ through ψ form a nonlinear, simultaneous first order set which is numerically integrated by the Adams method or by Gears method using a computed or a derived analytical Jacobian. The system is not stiff and all methods gave the same numerical results. Eight byte numerical precision was required for the computation.

More than 200 computations for different initial conditions in the phase space $\delta x_0\ \delta x_0'\ \delta y_0\ \delta y_0'$ were run to define the linear gain phase space acceptance of the FEL. δx_0 and $\delta x_0'$ are the displacement and angle of the input electron beam with respect to the reference wiggler orbit at the entrance plane and similarly for δy_0 and $\delta y_0'$ in the perpendicular plane. The wavelength 67.55 μm corresponds to maximum gain for the reference orbit. For the displaced orbits gain roll-off is the result of two distinguishable effects. An electron executing betatron oscillation enters regions of reduced optical field amplitude. The betatron oscillation also reduces the average axial velocity, detuning the resonance between the electron motion and the ponderomotive wave. For large deviations the resonance may cross from the gain region into an absorption region. The gain roll-off due to these two effects can be remarkably steep.

Contours of constant gain are plotted in fig. 3 at various intervals for the phase space defined by distance displacements $\delta x_0\ \delta y_0$ in the entrance plane. For this plot $\delta x_0' = \delta y_0' = 0$. The transformation $\delta y_0 \rightarrow -\delta y_0$ gives symmetric curves and there is a slight asymmetry associated with the transformation $\delta x_0 \rightarrow -\delta x_0$. At a radius 0.0002 m the gain roll-off is 10%.

Beam line matching problems are most often treated in the phase space planes $\delta x_0\ \delta x_0'$ and $\delta y_0\ \delta y_0'$. Since the $\delta x_0\ \delta x_0'$ plane corresponds to the wiggler direction it is more sensitive to orbit displacements. Also beam steering at the entrance to the wiggler will be dominated by the bend necessary in the wiggler plane. Gain contours are plotted in the $\delta x_0\ \delta x_0'$ phase space in fig. 4. The lower half of the plot is the mirror image of the upper half, to the accuracy of the plot execution. It is not exactly symmetric. The main information that may be read from this plot is the beam emittance required at the wiggler injection plane. For 1% gain roll-off, the normalized emittance is about 4 mm mrad, at 5% it is about 15 mm mrad and at 20% gain roll-off it is about 40 mm mrad. A distributed beam would require a weighted average over the phase space area. The normalized emittance is computed as γ times the phase area contained within the gain contour. The emittance at the wiggler entrance defines requirements for the electron optics in the entire accelerator section from the electron gun onward.

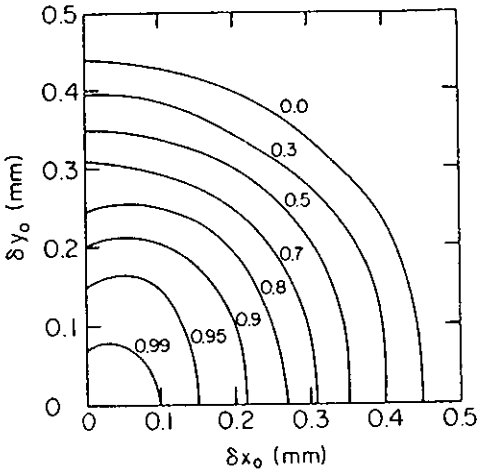

Fig. 3. Gain roll-off contours for displaced electron beams relative to the gain for the reference beam.

The beam recovery system acceptance has not yet been determined. At the time of writing, only pre-

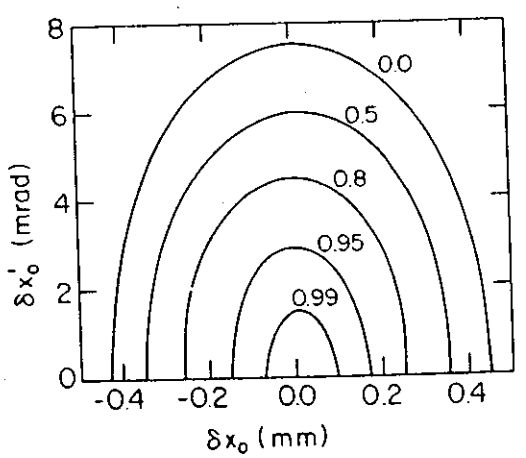

Fig. 4. Gain contours in the phase space of the wiggler plane.

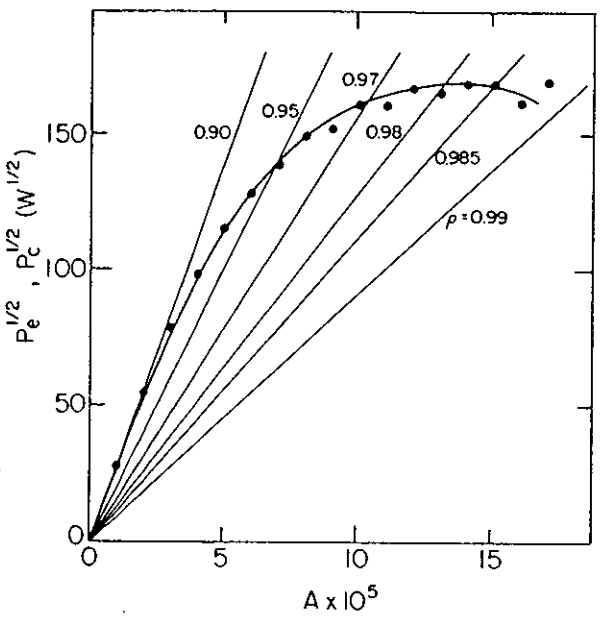

Fig. 5. Nonlinear saturation curve and cavity loss lines for various mirror reflection coefficients. Dots represent computed points.

liminary computations regarding the phase space spread in the FEL have been made. However, the gain saturation curve for single mode excitation has been determined. Fig. 5 shows the power transferred to the radiation field, P_e, at the wavelength corresponding to maximum nonlinear gain, as a function of the dimensionless radiation vector potential A. The gain saturation curve intersects cavity transmission loss lines, P_c, plotted for mirror power reflection coefficients ρ between 0.90 and 0.99. Intersections correspond to power balance in the saturated steady state.

Threshold oscillation is achieved for $\rho \geq 0.90$. Efficient generation of optical radiation should require $\rho \approx 0.96$ where the predicted output power is about 20 kW. The gain saturation curve intersects cavity loss lines at the field amplitudes of the saturated steady state. The importance of matching the nonlinear operating point to the beam optics of the beam recovery system is evident. At a high field amplitude the beam may exceed the phase space of the recovery system and the tandem accelerator may be unable to sustain the beam current.

References

[1] E. Jerby, A. Gover, S. Ruschin, H. Kleinman, I. Ben-Zvi, J.S. Sokolowski, S. Eckhouse, Y. Goren and Y. Shiloh (Sept. 86) Nucl. Instr. and Meth. A259 (1987) 263.
[2] L.R. Elias, R.J. Hu and G.J. Ramian, Nucl. Instr. and Meth. A237 (1985) 203.
[3] T.I. Smith and J.M.J. Madey, Appl. Phys. B27(1982)195.
[4] A. Gover and A. Friedman, The Optical Parameters of Free Electron Radiators, presented at 8th Free Electron Laser Conf., Glasgow, Scotland (Sept. 86).
[5] W.B. Herrmannsfeldt, SLAC-226 UC-28 (A), Stanford Linear Accelerator Center, Stanford California USA (1979).
[6] E.T. Scharlemann, Wiggle Plane Focusing in Linear Wigglers, J. App. Phys. 58 (6) (1985) 2154.
[7] H. Kogelnik and T. Li, Applied Optics 5 (10)(1966)1550.
[8] E. Jerby and A. Gover, Nucl. Instr. and Meth. A250 (1986) 192.